On the Role of Robot Configuration in Cartesian Stiffness Control

Arash Ajoudani, Nikos G. Tsagarakis, and Antonio Bicchi

Abstract— **The stiffness ellipsoid, i.e. the locus of task-space forces obtained corresponding to a deformation of unit norm in different directions, has been extensively used as a powerful representation of robot interaction capabilities. The size and shape of the stiffness ellipsoid at a given end-effector posture are influenced by both joint control parameters and - for redundant manipulators - by the chosen redundancy resolution configuration. As is well known, impedance control techniques ideally provide control parameters which realize any desired shape of the Cartesian stiffness ellipsoid at the end-effector in an arbitrary non-singular configuration, so that arm geometry selection could appear secondary. This definitely contrasts with observations on how humans control their arm stiffness, who in fact appear to predominantly use arm configurations to shape the stiffness ellipsoid.**

To understand this discrepancy, we provide a more complete analysis of the task-space force/deformation behavior of redundant arms, which explains why arm geometry also plays a fundamental role in interaction capabilities of a torque controlled robot. We show that stiffness control of realistic robot models with bounds on joint torques can't indeed achieve arbitrary stiffness ellipsoids at any given arm configuration. We first introduce the notion of maximum allowable Cartesian force/displacement ("stiffness feasibility") regions for a compliant robot. We show that different robot configurations modify such regions, and explore the role of different configurations in defining the performance limits of Cartesian stiffness controllers. On these bases, we design a stiffness control method that suitably exploits both joint control parameters and redundancy resolution to achieve desired task-space interaction behavior.

I. Introduction

Contact stability in humans and robots is guaranteed by generating task-adapted restoring forces in response to the environmental displacements, which can be achieved using different techniques. For instance, in humans, muscle activations can modify the joint stiffness matrix via cocontraction of muscles involved in the task [1], or through modifications in the sensitivity of reflex feedback [2]. Similarly in robots, the joint stiffness profile can be adjusted to realize a desired compliant behavior in Cartesian coordinates through conservative congruence transformations [3].

Endpoint stiffness in different directions, often represented by stiffness ellipsoids [4], [5], is also modified by varying the geometry of the arm; due to this geometric dependence, endpoint stiffness is subject to variations depending on the position of the endpoint in task space, or even on the arm configuration for the same end-effector position, when the arm is redundant [5].

Observations in human neuromotor control of the arm endpoint stiffness suggest that due to i) the major contribution of the limb geometry to efficient modifications in the orientation of the endpoint stiffness ellipsoid, ii) ergonomic efficiency of postural adjustments in comparison to cocontractions, and iii) the existence of cross–joint muscles in limbs, humans tend to maximize the use of limb postures to realize a desired endpoint stiffness direction [1]. Concurringly, cocontractions appear to mostly contribute to modifications in size, rather than orientation of the stiffness ellipsoid [6].

Relying on the above observations, the Common-Mode Stiffness (CMS) and Configuration Dependent Stiffness (CDS) concepts were previously introduced to describe the effect on end–point stiffness of uniformly stiffening all joints and of changing the redundancy resolution configuration, respectively [7], [8]. In these schemes, the CMS control implements a coordinated stiffening profile in robot joints and contributes to modification in size of the stiffness ellipsoid, with no or small effect on its shape. On the other hand, the CDS control regulates redundant joints of the robot arm to shape its stiffness ellipsoid according to the shape of the reference ellipsoid. Application of the CDS controller in the above referenced papers not only obtained good interaction control, but also generated rather natural motions, similar to the ones observed in humans executing similar tasks.

In general, CDS control can be usefully adopted to better approximate a desired Cartesian stiffness control under constraints on joint–space stiffness, as e.g. due to underactuation [7], [8], or to the use of decoupled joint stiffness control when using passive stiffness via Variable Stiffness Actuators (VSA) at the joints [9]. On the other hand, in a torque controlled robot (in which no such constraints are present), it is known [10] that in principle, any arbitrary endpoint stiffness matrix can be realized in any arbitrary configuration. With that being said, the CDS control might appear secondary. However, to realize an arbitrary stiffness matrix, the desired endpoint force/displacement relationship must be mathematically mapped to the joint–space (cf. e.g. (2) below), which requires in general that the torque commanded at any joint depends on the robot geometry and the displacement of all joints in a tightly coupled way [11], [12].

To investigate the effect of robot configuration on task-force capabilities, force ellipsoid was initially introduced in [13] as the preimage of the unit sphere in the joint torque space under a mapping which is defined by the robot

Arash Ajoudani, Nikos G. Tsagarakis and Antonio Bicchi are with the Dept. of Advanced Robotics, Istituto Italiano di Tecnologia, Via Morego 30, 16163, Genova, Italy. Arash Ajoudani and Antonio Bicchi are also with Interdepartmental Research Center "E. Piaggio", Faculty of Engineering, University of Pisa, Italy. e-mails: arash.ajoudani@iit.it, nikos.tsagarakis@iit.it and bicchi@centropiaggio.unipi.it.

This work is supported in part by the European Research Council under the Advanced Grant SoftHands, no. ERC-291166, and EU FP7-ICT project, WALK-MAN, no. 611832.

geometry. Thereafter, the concept has been adapted to suit to different tasks and platforms (e.g. see [14]). Notwithstanding the widespread use of force ellipsoids, they are known to be imprecise due to the fact that in such a representation the dynamic boundaries, i.e. the actuators' torque limits, are not taken into account. As an alternative solution, the use of force polytopes were recommended that account for exact maximum achievable task space force, subject to the imposed constraints in the space of joint torques [15].

It is important to note here that both the above representations only convey a local picture of the manipulator's capabilities. In a compliant robot, where the aim is to realize a desired Cartesian stiffness matrix, applied external displacements will modify the robot configuration, and the realized force polytopes as a consequence. This means that the maximum allowable deviation in the space of Cartesian displacements will be defined by the initial configuration, the desired task force profile and the boundaries in the space of joint torques. One of the objectives of this paper is to address this problem and demonstrate that the Cartesian force boundary of a compliant robot in an arbitrary configuration has a nonpolytopic shape in general. In addition, a dual but more intuitive representation of such a performance limit is presented in the space of Cartesian displacements.

Now assume that a Cartesian stiffness controller in a torque controlled robot is implemented to realize a desired stiffness matrix, in a particular configuration. This is associated with a maximum allowable displacement region, after reaching which, some actuators will hit the boundaries in the space of joint torques and the equilibrium assumption will no longer be valid. As a consequence, realization of the stiffness matrix will be subject to uncertainty. Noteworthy, the actuators' torque saturation under the Cartesian stiffness control will occur later for some configurations than for others: this is the next topic we would like to investigate and capture with our measure. Here, the desired interaction performance is defined by realizing the "best" boundary region in Cartesian coordinates that correspond to the maximum allowable deviation form the initial equilibrium point. We demonstrate that even though a torque controlled robot in an arbitrary configuration is capable of realizing any shape of the stiffness ellipsoid at the end-effector, particular joint geometry renders the best interaction performance compared to the others, demonstrating the underlying concept in the alternative usage of the CDS in Cartesian stiffness control.

II. Performance Limits of the Cartesian Stiffness Control – Nonredundant Case

Consider the robot with forward kinematic map $x = \Lambda(q)$ initially at equilibrium $E(q_0, \tau_0, f_0)$ with $x_0 = \Lambda(q_0)$ and $\tau_0 = J^T(q_0) f_0$, and a nearby equilibrium $E(q, \tau, f)$, with $x = \Lambda(q)$ and $\tau = J^T(q) f$. Here, x, f, q, and τ denote the Cartesian position/orientation, Cartesian force, joint angle, and joint torque vectors, respectively. $J \in \mathbb{R}^{m \times n}$ is the manipulator Jacobian with n being the number of joints and m corresponding to the task space dimension.

Let $q = q_0 + \delta q$, $f = f_0 + \delta f$, and $\tau = \tau_0 + \delta \tau$, and assume that the aim is to realize a desired force profile in the task space, hence $\delta f = F(\delta x, x_0)$, with F being an unknown function. By taking a first order Taylor expansion, we obtain

$$\begin{aligned} \tau_0 + \delta\tau &= J^T(q_0+\delta q)\,(f_0+\delta f) \\ &= J^T(q_0+\delta q) f_0 + J^T(q_0+\delta q)\delta f \\ &\approx J^T(q_0) f_0 + \left.\frac{\partial J(q)^T f_0}{\partial q}\right|_{q_0} \delta q + J^T(q_0)\delta f \\ &+ \left.\frac{\partial J(q)^T \delta f}{\partial q}\right|_{q_0} \delta q, \end{aligned} \tag{1}$$

with the last term in the above equation being negligible,

$$\delta\tau = J^T(q_0)\delta f + \left.\frac{\partial J^T f_0}{\partial q}\right|_{q_0} \delta q.$$

The fundamental idea behind the stiffness control is to realize a control law $\delta\tau$ such that for a given kinematics $\Lambda(q)$, the desired Cartesian force function f is realized. In general, determining such a function is not easy. However, this can be done using 1st-order approximations, i.e. $\delta f = K_c \delta x$, where $x = x_0 + \delta x = \Lambda(q_0 + \delta q)$ and K_c denotes the stiffness matrix. Thus, the corresponding torque to be commanded at the joints is

$$\delta\tau = J^T(q_0) K_c \delta x + \left.\frac{\partial J(q)^T f_0}{\partial q}\right|_{q_0} \delta q. \tag{2}$$

Note that the above equation is only valid for small displacements around the initial equilibrium point. For a relatively large deformation of the nonredundant manipulator's end-effector, the generally nonlinear association between the manipulator's joint torque and Cartesian force vector can be represented by a series of relinearized equations for each nearby equilibrium pair within the continuous closed interval[1] $[x_0\ x_1\ \cdots\ x_k\ \cdots\ x_{n_{eq}}]$, with $\tau_i = J^T(q_i) f_i$, and $i \in \mathbb{R}^{n_{eq}}$. Using a similar technique as in (1) and (2), at each step, the supplementary joint torque can be calculated using the current measurements as follows

$$\delta\tau_k = J^T(q_{k-1}) K_c \delta x_k + \left.\frac{\partial J(q)^T f_{k-1}}{\partial q}\right|_{q_{k-1}} \delta q_k, \tag{3}$$

with $k-1$ and k denoting the index numbers which correspond to the two nearby equilibriums. Equation (3) must comply with the maximum achievable task space forces and velocities for given limits in the joint space[2] [17]. Otherwise, certain values of external disturbance will cause torque saturation and as a consequence, the equilibrium condition assumption will no longer be valid and the realized stiffness behavior will not be desired.

To illustrate the underlying concept, let's consider a two-link manipulator in configuration A as depicted in Fig. 1, left plot. Assume that the aim is to realize a desired stiffness matrix $K_{c_d} = \begin{bmatrix} 1 & 0.2 \\ 0.2 & 2 \end{bmatrix} \frac{kN}{m}$, at the end-effector of the robot. For small values of δy along the negative direction, restoring

[1] Assuming that no singularity occurs in this boundary and the final point $x_{n_{eq}}$ is reachable.

[2] In this paper we only consider the dynamic boundaries of the robot. A detailed discussion on the mobility and manipulability of the robots regarding kinematic constraints can be found in [16].

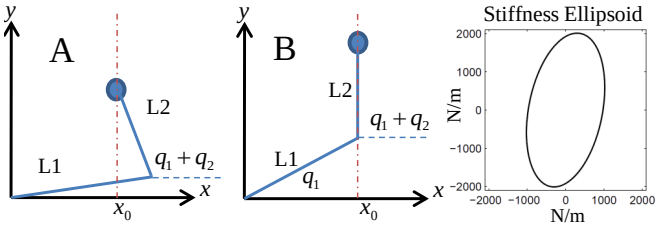

Fig. 1: Two-link manipulator in configuration A (left) and B (middle). $q_A = [10^o, 110^o]$, $q_B = [31^o, 59^o]$, $L_1 = 0.14\,m$, $L_2 = 0.12\,m$, $|\tau_1| \leq 3\ Nm$, and $|\tau_2| \leq 2\ Nm$. Desired stiffness ellipsoid is plotted on the most right.

forces will demonstrate a linear trend. However, at a certain point (y = y_A, see Fig. 2), the actuator torque will saturate and from this point on, the force-displacement relation will not satisfy the equilibrium condition and the realized task stiffness will not be desired.

Now, consider the same manipulator in another configuration (B, Fig. 1, middle plot), exposed to a similar external displacement profile. In this configuration, joint torques will hit the limits at y = $y_B > y_A$, highlighting the fact that the actuation torque saturation while realizing a desired compliant profile will happen later for some configurations than for others.

Force capabilities of the manipulator in a given configuration is classically represented by the force manipulability ellipsoid [13], and is defined as the image of the unit sphere in the joint torque space, i.e.

$$\tau^T \tau \leq 1 \ \Rightarrow \ f^T J(q) J^T(q) f \leq 1.$$

Directions and magnitudes of the principal axes of the force ellipsoid correspond to the eigenvectors and (reciprocal of) eigenvalues of $J(q)$, respectively. It is well known that such a graphical representation does not fully illustrate the force capabilities of the manipulator since boundary limits in the space of joint torques are not taken into account. Alternatively, the concept of force polytopes was introduced in [15] to address the maximum achievable task space force profile that comply with manipulator's torque polytopic boundary. If the manipulator is nonredundant (i.e. $J(q)$ is full rank if not singular), due to the linearity of the mapping between the joint and Cartesian space and the convex properties of the torque polytopes, resulting force polytopes are also convex with vertices being the images of the vertices of the torque polytopes under the $J^{-T}(q)$ mapping. However, such a property only holds under the assumption that the manipulator configuration is fixed. In other circumstances such as tracking a desired task space stiffness profile, applied external displacements will alter the manipulator configuration, and the task space force boundaries of the manipulator as a consequence. This conveys that for any initial equilibrium point in workspace, the force/displacement boundary region has a non-polytopic shape in general. Traditional force polytope is only a linear estimate of such a region, while the force ellipsoid is even less accurate.

To realize a desired compliant profile at the end-effector of a robot, efficient restoring forces must be generated in

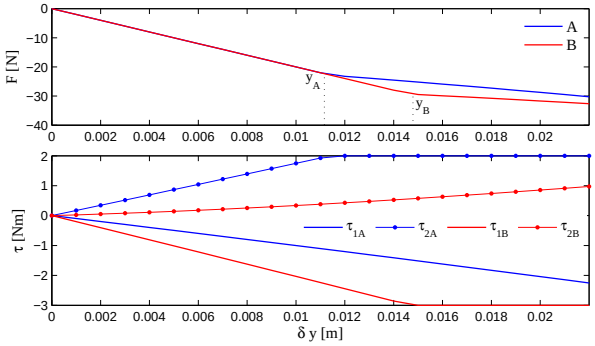

Fig. 2: Endpoint forces vs. displacements along $-y$ direction in manipulators A and B (upper plot), and the corresponding joint torques (lower plot).

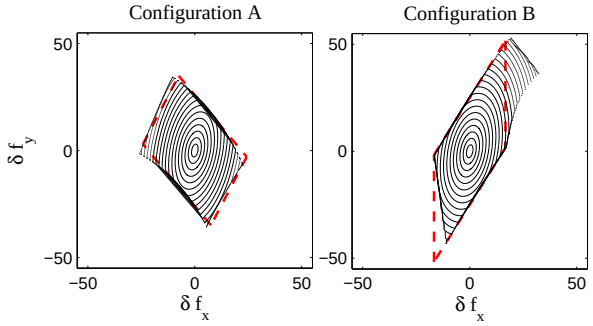

Fig. 3: The locus of $||f||$ for the growing displacement norm for the two-link manipulator in configuration A (left plot), and B (right plot) hit the limits caused by two configuration dependent force boundaries. Traditional force polytopes are also plotted for each configuration in red.

response to environmental displacements. Traditionally, the stiffness ellipsoid is defined as the locus of forces obtained $||f||$, corresponding to a deformation of unit norm. The directions of the principal axes of the stiffness ellipsoid are given by the set of orthonormal output vectors of the singular value decomposition (SVD) of this ratio, while their magnitudes are given by reciprocal of the corresponding singular values. It is important to note that stiffness ellipsoid only conveys a "local" picture of operational stiffness, i.e. for small forces and displacements. If larger displacements are applied, however, at a certain point the manipulator will get out of the feasibility polytope in joint torques. Thus, for a displacement profile with a growing norm, we will realize families of growing force ellipsoids which at some point will get cut by a boundary region at different places.

Considering our two-link example in Fig. 1, we calculate and plot the stiffness ellipsoid for K_{c_d} (see Fig. 1, most right plot). On the other hand, if we plot the locus of $||f||$ for the desired Cartesian stiffness matrix and different scales of the unit circle displacement profile, we realize that the ellipsoids are cut by two non-polytopic profiles corresponding to the task space force boundaries of the manipulator in configurations A and B (Fig. 3, left and right plot, respectively). For the sake of comparison, classical force polytopes are also plotted in red (dashed).

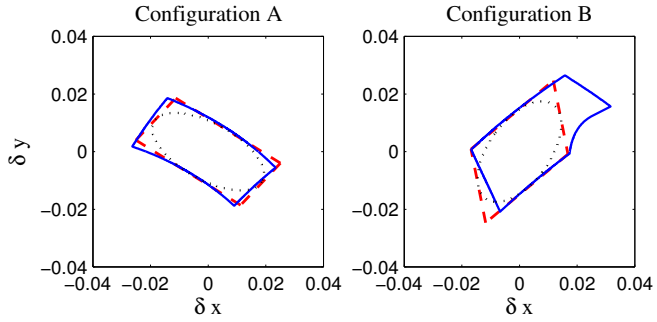

Fig. 4: Blue (solid) plots illustrate the SFRs for configuration A (left) and B (right), while corresponding polytopes are plotted in red (dashed). SFEs are plotted in black (dotted), for both configurations.

A. Stiffness Feasibility Region

Stiffness feasibility region (SFR) is here defined by a boundary (non-polytopic in general) in the space of Cartesian displacement (or force as a dual representation) that correspond to the maximum allowable deviation (external force) from the initial equilibrium point, where within this boundary, the realization of the desired Cartesian stiffness matrix is feasible. Overreaching this boundary signifies that at least one of the actuators has hit the limits in the space of joint torques and as a consequence, the realization of the desired stiffness matrix will be subject to uncertainty. Fig. 4 demonstrates SFRs of the two link manipulator in configuration A (left) and B (right) for K_{c_d}, mentioned above.

It is important to note that although SFRs provide accurate representation of the imposed performance limits while realizing a desired stiffness matrix, their calculation is computationally expensive. In particular, concerning redundant manipulators, described in the following sections, both representations (SFR and stiffness feasibility polytopes (SFP)) require several steps to account for the task space boundary regions. To that end, we propose and calculate the stiffness feasibility ellipsoids (SFE), a fast and intuitive, but local estimate of the stiffness feasibility regions.

To do so, a proper scaling of the joint torques due to the imposed actuator boundaries[3] is defined by $\hat{\tau} = W_\tau \tau$, with $W_\tau = \text{diag}[\frac{1}{\tau_{lim_1}} \; \frac{1}{\tau_{lim_1}} \; \dots \; \frac{1}{\tau_{lim_n}}]$, and τ_{lim_i} denoting the torque limit of the joint number i, that is $|\tau_i| \leq \tau_{lim_i}$. Thus

$$\tau^T W_\tau W_\tau \tau \leq 1 \;\Rightarrow\; f^T J(q) W_\tau W_\tau J^T(q) f \leq 1, \qquad (4)$$

which under the mapping in (2) becomes

$$\delta x^T K_c J(q) W_\tau W_\tau J^T(q) K_c \delta x \leq 1. \qquad (5)$$

The set of orthonormal outputs of the SVD of $K_c J(q) W_\tau$ indicate the direction of the principal axes of the SFE, with the magnitudes calculated by the reciprocal of the corresponding eigenvalues. Such ellipsoids for the two-link example are plotted in Fig. 4 in black (dotted).

Above discussions highlight the fact that even though any desired task-space stiffness matrix can be realized via a Cartesian stiffness controller, the feasibility of realizing such a profile under higher external forces/displacements requires a predictive control of the manipulator configuration.

III. Performance Limits of the Cartesian Stiffness Control – Redundant Case

It is well known that for a redundant manipulator, the transformation between the joint and task spaces does not ensure the uniqueness of the solution for the task space forces [17]. Minimization of the norm $\|\tau - J^T(q) f\|$ is commonly carried out by using the pseudo-inverse solution, that is $f = J^+(q)\tau$. However, the only condition ensuring that this norm equals zero, is that all joint torques are associated to the image of the Jacobian transpose. For this reason, to account for the task space performance limits of the redundant manipulator for a given torque boundary, only vector of joint torques that do not generate internal motions must be taken into account. This will produce reduced force boundary region, which is basically the intersection of the joint torque boundary region with the image of $J^T(q)$.

An algorithm is proposed in [17] to account for the force manipulability polytope in a certain configuration of a redundant robot. This is important, however, to note here that this algorithm estimates for the reduced force manipulability polytope for a fixed end-effector position in the Cartesian space. Once the robot configuration is altered (e.g. under external disturbance), the corresponding force polytope must be recalculated. This results in a generally non-polytopic shape, while sweeping the Cartesian space to appoint to the boundary region of the task force/displacement.

Another issue in computation of the force boundary region for a redundant manipulator is that any applied displacement in the task space can be transformed into non-unique solutions in the space of joint velocities. This indicates that the chosen policy regarding the update of the joint velocities can potentially revise the resulting performance limits of the Cartesian stiffness control to realize a task-appropriate size and/or isotropy of the SFR.

A. Stiffness Feasibility Region - Redundant Case

As mentioned earlier, SFE is a fast but somewhat inaccurate tool that conveys some intuitive information on the space of maximum allowable deviation from the initial equilibrium point of a compliant robot. Especially, the direction of the maximum allowable displacement and the isotropy index (ratio between the maximum and the minimum axis [18]) of the ellipsoid are profitable properties which can be potentially used to define and realize a desired performance through the predictive control of the configuration.

To visualize the SFE for a redundant manipulator, the unit sphere in joint torque space is transformed into the task space and it's intersection with the image of the Jacobian transpose is calculated. It is well known that such a transformation can be performed by J^+J which leads to a similar equation as in (5), for a redundant manipulator[4], since $JJ^+JJ^T = JJ^T$.

[3] Antisymmetric boundaries of the joint torques can be treated with a proper mapping to result in a symmetric inequality [16].

[4] The torque antisymmetry scaling can be performed by introducing the scaled Jacobian as $\tilde{J}^T(q) = W_\tau J^T(q)$ [17].

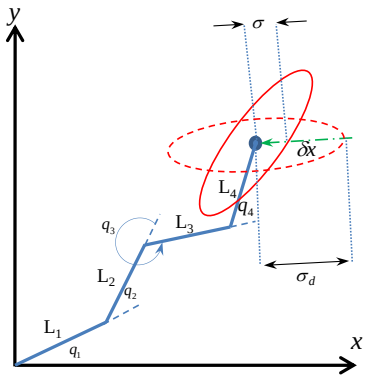

Fig. 5: 4-link planar manipulator. The SFEs are plotted in solid and dashed which correspond to a similar Cartesian stiffness matrix, but different interaction performances regarding the task space boundaries (see text for details).

IV. Increased Performance of the Cartesian Stiffness Controller through Optimal Redundancy Resolution

It was shown that the SFRs for both redundant and non-redundant manipulators strongly depend on the manipulator configuration and the desired stiffness matrix. This points to the task dependency of the to be utilized optimization algorithm to adjust the configuration of the robot and render a desired performance. For instance, the redundant joints of the robot can be controlled in a way to realize the most isotropic shape or biggest size of this region. In this direction, we propose and implement an on-line strategy to possibly align the "best" direction of the stiffness feasibility region with the applied external disturbance.

Consider a redundant robot with the aim to realize a desired Cartesian stiffness matrix K_{c_d}, subject to a certain boundary in the space of joint torques. To achieve this, the desired joint torque vector τ_d is calculated by

$$\tau_d = \tau_{c_d} + \tau_{N_d}, \tag{6}$$

with τ_{c_d}[5] and τ_{N_d}, corresponding to the Cartesian stiffness and nullspace torque vectors, respectively.

Now assume that a disturbance profile in a particular direction δx, is being applied to the end effector of the robot in a certain configuration (e.g. the four-link planar robot as depicted in Fig. 5, with the SFE depicted in red (solid line)). A desired orientation of the SFE can be illustrated by coinciding the major axis of the realized SFE (dashed line, $\sigma = \sigma_d$) with the direction of the applied displacement. To achieve this, we calculate the maximum, locally allowable displacement σ, along the direction of the external displacement $\frac{\delta x}{\|\delta x\|}$, on the SFE

$$[\sigma \frac{\delta x}{\|\delta x\|}]^T K_c J(q) W_\tau^2 J^T(q) K_c [\sigma \frac{\delta x}{\|\delta x\|}] = 1, \tag{7}$$

with $\|.\|$ denoting the vector norm operator. Solving for σ we obtain

$$\sigma = [\frac{\delta x^T}{\|\delta x\|} K_c J(q) W_\tau^2 J^T(q) K_c \frac{\delta x}{\|\delta x\|}]^{\frac{-1}{2}}. \tag{8}$$

[5]Details of the implementation of τ_{c_d} can be found in [10].

The nullspace torque vector can be adjusted to re-orient the major axis of the SFE towards the direction of $\frac{\delta x}{\|\delta x\|}$. To do so, τ_{N_d} is calculated by projecting the gradient of the cost function

$$V = \sum_{i=1}^{l} w_i {\sigma_i}^2 \tag{9}$$

into a dynamically consistent nullspace of the Jacobian transpose [19],

$$\delta\tau_{N_d} = [I - J^T(q)\tilde{J}^T(q)] \frac{\partial V(q)}{\partial q}, \tag{10}$$

where I, l and w denote the identity matrix, considered number of axes in the SFE and the corresponding scale, respectively. $\tilde{J}(q)$ can be defined using the mass matrix $M(q)$, as follows

$$\begin{aligned} \tilde{J}(q) &= M^{-1}(q)\, J^T(q)\, \hat{M}(q), \\ \hat{M}(q) &= [J(q)\, M^{-1}(q)\, J^T(q)]^{-1}. \end{aligned} \tag{11}$$

Eventually, to be commanded joint motor torque τ_m, can be calculated as

$$\tau_m = \tau_d - K_\tau(\tau - \tau_d) - K_{\dot{\tau}}\dot{\tau} \tag{12}$$

with positive definite controller matrices K_τ and $K_{\dot{\tau}}$, and $\dot{\tau}$ denoting the torque derivative. It has been demonstrated that the implementation of (12) can stabilize the torque dynamics around the equilibrium point $\tau = \tau_{d_k}$ [10], with τ_{d_k} being updated using (3) and (10).

V. Results

A. Simulation Results: Four Link Manipulator

In this section, we evaluate the efficiency of the proposed algorithm for the 4-link planar redundant robot in Fig. 5. The aim is to realize a desired Cartesian stiffness matrix, subject to specific boundaries in the space of joint torques: $|\tau_1| \leq 5\ Nm$, $|\tau_2| \leq 4\ Nm$, $|\tau_3| \leq 3\ Nm$, and $|\tau_4| \leq 2\ Nm$. $K_{c_{des}}$ is considered similar to the 2-link example. Links are assumed to have the same length, that is $0.2m$. The position of the end effector is assumed to be fixed on the plane.

Starting from any initial configuration (Fig. 6, dashed plots), for a given external disturbance vector, (δx, Fig. 6, green arrows), and $K_{c_{des}}$, the manipulator configuration is adjusted (Fig. 6, solid plots) to possibly align the initial SFE (Fig. 6, blue-dotted) with the desired one (Fig. 6, red-solid). As a result, even if the Cartesian stiffness profile is equal for all configurations, the optimized configurations provide more efficient interaction performance, meaning that the joint torque actuation saturation will occur for larger external displacements/forces, compared to the starting configurations. Figs. 7. a and b illustrate the calculated SFRs for configurations A and D of Fig. 6, respectively. The blue (dashed) regions correspond to the initial configuration, while the solid (black) ones are realized consequent to the optimization of the redundancy. A comparison between Fig. 6 and Fig. 7 illustrates that directions of the maximum allowable displacement in SFRs agreeably coincide with the ones in the corresponding SFEs.

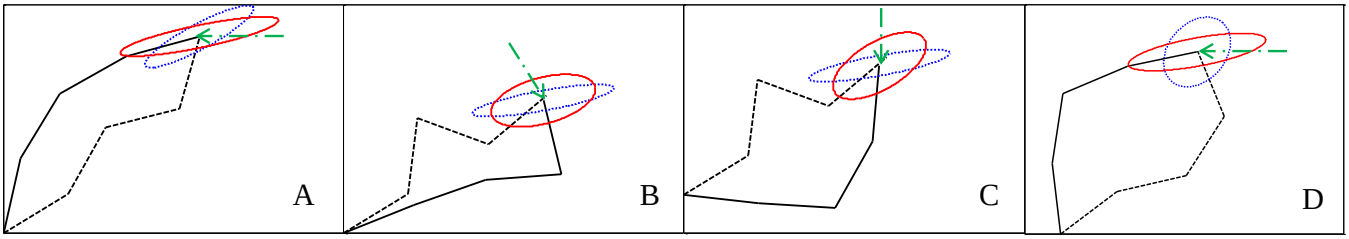

Fig. 6: Initial (dashed) and optimized (solid) configurations and SFEs of the four link example to render the best performance for the disturbance profile applied along a specific direction. The optimization algorithm utilizes the direction of the maximum SFE to orient the boundary region towards the direction of the applied disturbance.

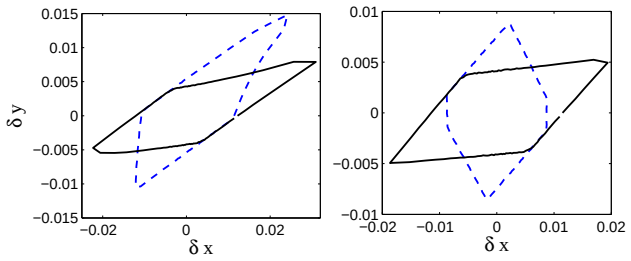

Fig. 7: Stiffness feasibility regions for initial (blue, dashed) and final (black, solid) configurations A(a) and D(b) in Fig. 6. In both plots the external disturbance is assumed to be applied along x direction.

B. Simulation Results: Compliant Humanoid Robot

In this section, the efficiency of the proposed controller in rendering a desired interaction performance is evaluated on a compliant humanoid robot arm COMAN [20]. A model of the COMAN robot is developed and simulated in Gazebo (http://gazebosim.org). In our simulation model, to highlight more the effect of configuration control during interaction, the joint torque limits were considered one third of the nominal values. Details of the kinematic and dynamic models of the robot and the utilized interfaces for joint torque/impedance/position control can be found in [21]. A postural task is defined to track a desired position and orientation of the left arm in the workspace (Fig. 8, left side). A diagonal desired stiffness matrix, with $[2.5\ 2.5\ 2.5\ 0.25\ 0.25\ 0.25]\frac{kNm}{rad}$, being the stiffness values along the main diagonal is tracked by the proposed Cartesian stiffness controller. Consequently, various displacement profiles were implemented and applied to the left hand of the COMAN robot.

A typical result of the proposed redundancy resolution for improved interaction performance is illustrated in Fig. 8, right side. In this example, an external displacement profile along y direction (the yellow/dashed vector) is applied to the left hand of the robot. Corresponding SFRs for both configurations in xy plane are demonstrated in Fig. 9. As observed in these plots, an efficient elongation of the SFR towards the external disturbance vector is achieved, even if only one degree of redundancy is available for this fully constrained task. Optimized configuration provides bigger displacement region along the direction of the disturbance while realizing the desired stiffness matrix. Outside of the

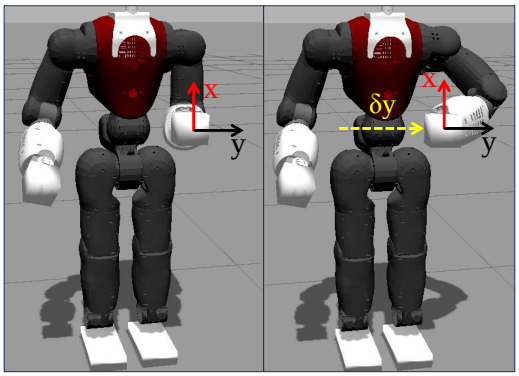

Fig. 8: COMAN robot in the initial configuration on left. The arm configuration (right side) has been optimized (consequent to the optimization of τ_{N_d}) to re-orient the direction of the major axis of the realizes SFE towards the direction of the applied external disturbance (y direction, yellow/dashed). Observed behavior looks natural.

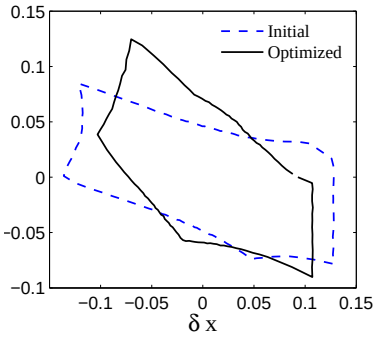

Fig. 9: Stiffness feasibility regions for initial (blue, dashed) and optimized (black, solid) configurations of Fig. 8, projected in xy plane. In this example, the displacement profile is along y direction.

corresponding regions, at least one of the arm joints will hit the joint torque limit boundary and as a consequence, realization of the desired Cartesian stiffness matrix will be subject to uncertainty.

C. Experimental Results

Preliminary experiments were carried out to further evaluate the efficiency of the proposed interaction controller. A Cartesian impedance controller was developed for KUKA lightweight robot to realize a diagonal stiffness matrix with $3\ \frac{kN}{m}$ and $0.3\ \frac{kNm}{rad}$ being the translational and rotational components. Once an external disturbance is applied (e.g. along y direction), the proposed algorithm optimizes the

redundant degrees of freedom from an initial configuration (e.g. Fig. 10, left side) to a configuration (Fig. 10, right side) in which the realized SFR is elongated more towards the external disturbance. Fig. 11 illustrates the achieved initial (blue) and optimal (red) SFPs for this experiment. Dark to light grey plots demonstrate geometric variations of SFPs while the null space torque vector drives the redundant dof towards the optimal configuration.

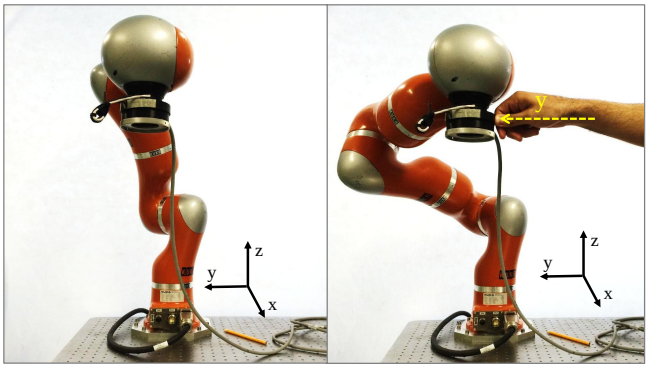

Fig. 10: KUKA robot in initial (left side) and optimized (right side) configurations.

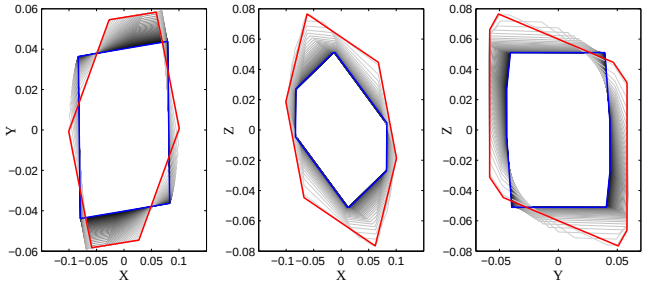

Fig. 11: Experimental verification of the proposed control law in extending the realized SFR towards the direction of applied disturbance (y). SFP is projected into xy, xz, and yz planes for initial (blue) and final (red) configurations (units in meters). Color map from black to light grey demonstrates the geometric variations of the realized SFP, consequent to the iterative redundancy resolution.

VI. Conclusions

In this paper, we provided a detailed analysis of the task-space force/deformation behavior of redundant arms to explain why arm geometry plays a fundamental role in interaction capabilities of a torque controlled robot. We demonstrated that due to the imposed boundaries in the space of joint torque, we can't indeed realize an arbitrary stiffness ellipsoids at any given arm configuration. In this direction, we introduced the notion of maximum allowable Cartesian force/displacement ("stiffness feasibility") regions for a compliant robot and demonstrated that different robot configurations modify such regions. Eventually, a control framework to realize a task-appropriate stiffness feasibility region by optimizing the redundancy was proposed and experimentally evaluated.

References

[1] T. Milner, "Contribution of geometry and joint stiffness to mechanical stability of the human arm," *Experimental Brain Research*, vol. 143, pp. 515–519, 2002.

[2] K. Akazawa, T. Milner, and R. Stein, "Modulation of reflex EMG and stiffness in response to stretch of human finger muscle," *Journal of Neurophisiology*, vol. 49, pp. 16–27, 1983.

[3] S.-F. Chen and I. Kao, "Conservative congruence transformation for joint and cartesian stiffness matrices of robotic hands and fingers," *The International Journal of Robotics Research*, vol. 19, no. 9, pp. 835–847, 2000.

[4] J. K. Salisbury and J. J. Craig, "Articulated hands: Force control and kinematic issues," *The International Journal of Robotics Research*, vol. 1, no. 1, pp. 4–17, 1982.

[5] F. Mussa-Ivaldi, N. Hogan, and E. Bizzi, "Neural, mechanical, and geometric factors subserving arm posture in humans," *Journal of Neuroscience*, vol. 5, no. 10, pp. 2732–2743, 1985.

[6] A. Ajoudani, N. G. Tsagarakis, and A. Bicchi, "Tele-Impedance: Teleoperation with impedance regulation using a body-machine interface," *International Journal of Robotics Research*, vol. 31(13), pp. 1642–1655, 2012.

[7] A. Ajoudani, M. Gabiccini, N. G. Tsagarakis, A. Albu-Schäffer, and A. Bicchi, "TeleImpedance: Exploring the role of common-mode and configuration-dependant stiffness," in *IEEE International Conference on Humanoid Robots*, 2012.

[8] A. Ajoudani, N. Tsagarakis, J. Lee, M. Gabiccini, and A. Bicchi, "Natural redundancy resolution in dual arm manipulation through configuration dependent stiffness (cds) control," in *International Conference of Robotics and Automation - ICRA*, 2014.

[9] A. Albu-Schaffer, M. Fischer, G. Schreiber, F. Schoeppe, and G. Hirzinger, "Soft robotics: what cartesian stiffness can obtain with passively compliant, uncoupled joints?" in *IEEE/RSJ International Conference on Intelligent Robots and Systems*, 2004.

[10] A. Albu-Schaffer, C. Ott, U. Frese, and G. Hirzinger, "Cartesian impedance control of redundant robots: Recent results with the dlr-light-weight-arms," in *IEEE International Conference on Robotics and Automation*, 2003.

[11] A. Pashkevich, A. Klimchik, and D. Chablat, "Enhanced stiffness modeling of manipulators with passive joints," *Mechanism and machine theory*, vol. 46, no. 5, pp. 662–679, 2011.

[12] C. Huang and I. Kao, "Geometrical interpretation of the cct stiffness mapping for serial manipulators," in *Robotics Research*. Springer, 2003, pp. 419–431.

[13] T. Yoshikawa, "Manipulability of robotic mechanisms," *The international journal of Robotics Research*, vol. 4, no. 2, pp. 3–9, 1985.

[14] P. Chiacchio, S. Chiaverini, L. Sciavicco, and B. Siciliano, "Global task space manipulability ellipsoids for multiple-arm systems," *IEEE Transactions on Robotics and Automation*, vol. 7, no. 5, pp. 678–685, 1991.

[15] T. Kokkinis and B. Paden, "Kinetostatic performance limits of cooperating robot manipulators using force-velocity polytopes," in *Proceedings of the ASME Winter Annual Meeting*, 1989, pp. 151–155.

[16] A. Bicchi, C. Melchiorri, and D. Balluchi, "On the mobility and manipulability of general multiple limb robots," *Robotics and Automation, IEEE Transactions on*, vol. 11, no. 2, pp. 215–228, 1995.

[17] P. Chiacchio, Y. Bouffard-Vercelli, and F. Pierrot, "Force polytope and force ellipsoid for redundant manipulators," *Journal of Robotic Systems*, vol. 14, no. 8, pp. 613–620, 1997.

[18] J. Angeles and C. S. López-Cajún, "Kinematic isotropy and the conditioning index of serial robotic manipulators," *The International Journal of Robotics Research*, vol. 11, no. 6, pp. 560–571, 1992.

[19] O. Khatib, "Motion/force redundancy of manipulators," in *Proceedings of Japan-USA Symposium on Flexible Automation*, vol. 1, 1990, pp. 337–342.

[20] N. G. Tsagarakis, S. Morfey, G. Medrano Cerda, L. Zhibin, and D. G. Caldwell, "Compliant humanoid coman: Optimal joint stiffness tuning for modal frequency control," in *IEEE Robotics and Automation (ICRA)*, 2013.

[21] A. Ajoudani, J. Lee, A. Rocchi, M. Ferrati, E. M. Hoffman, A. Settimi, D. Caldwel, A. Bicchi, and N. Tsagarakis, "A manipulation framework for compliant humanoid coman: Application to a valve turning task," in *IEEE International Conference on Humanoid Robots*, 2014.